

RESEARCH ARTICLE

10.1002/2015JA021429

Key Points:

- During a large geomagnetic storm trapped outer radiation belt electrons were enhanced
- A gradual decay of the trapped fluxes was observed over the following 5–7 days
- Weak electron precipitation driven by dayside plasmaspheric hiss caused the decay

Correspondence to:

M. A. Clilverd,
macl@bas.ac.uk

Citation:

Hardman, R., M. A. Clilverd, C. J. Rodger, J. B. Brundell, R. Duthie, R. H. Holzworth, I. R. Mann, D. K. Milling, and E. Macusova (2015), A case study of electron precipitation fluxes due to plasmaspheric hiss, *J. Geophys. Res. Space Physics*, 120, 6736–6748, doi:10.1002/2015JA021429.

Received 6 MAY 2015

Accepted 16 JUN 2015

Accepted article online 19 JUN 2015

Published online 7 AUG 2015

A case study of electron precipitation fluxes due to plasmaspheric hiss

Rachael Hardman¹, Mark A. Clilverd¹, Craig J. Rodger², James B. Brundell², Roger Duthie¹, Robert H. Holzworth³, Ian R. Mann⁴, David K. Milling⁴, and Eva Macusova⁵

¹British Antarctic Survey (NERC), Cambridge, UK, ²Department of Physics, University of Otago, Dunedin, New Zealand, ³Departments of Earth and Space Sciences, University of Washington, Seattle, Washington, USA, ⁴Department of Physics, University of Alberta, Edmonton, Alberta, Canada, ⁵Department of Space Physics, Institute of Atmospheric Physics, Prague, Czech Republic

Abstract We find that during a large geomagnetic storm in October 2011 the trapped fluxes of >30 , >100 , and >300 keV outer radiation belt electrons were enhanced at $L = 3-4$ during the storm main phase. A gradual decay of the trapped fluxes was observed over the following 5–7 days, even though no significant precipitation fluxes could be observed in the Polar Orbiting Environmental Satellite (POES) electron precipitation detectors. We use the Antarctic-Arctic Radiation-belt (Dynamic) Deposition-VLF Atmospheric Research Konsortium receiver network to investigate the characteristics of the electron precipitation throughout the storm period. Weak electron precipitation was observed on the dayside for 5–7 days, consistent with being driven by plasmaspheric hiss. Using a previously published plasmaspheric hiss-induced electron energy e -folding spectrum of $E_0 = 365$ keV, the observed radio wave perturbation levels at $L = 3-4$ were found to be caused by >30 keV electron precipitation with flux ~ 100 el $\text{cm}^{-2} \text{s}^{-1} \text{sr}^{-1}$. The low levels of precipitation explain the lack of response of the POES telescopes to the flux, because of the effect of the POES lower sensitivity limit and ability to measure weak diffusion-driven precipitation. The detection of dayside, inner plasmasphere electron precipitation during the recovery phase of the storm is consistent with plasmaspheric hiss wave-particle interactions and shows that the waves can be a significant influence on the evolution of the outer radiation belt trapped flux that resides inside the plasmopause.

1. Introduction

During geomagnetic storms the flux of energetic electrons trapped in the outer radiation belt ($L = 3-8$) often increases but can also decrease [Reeves *et al.*, 2003]. During the same events energetic electron precipitation flux into the atmosphere typically intensifies over a large range of geomagnetic latitudes with significant fluxes over a range of energies [Neal *et al.*, 2015]. The overall dynamics of the outer radiation belt is a delicate interplay between source, transport, and loss processes, all of which are amplified during geomagnetic storms [Thorne *et al.*, 2005; Xiao *et al.*, 2014, and references therein]. Part of the complexity of this process is the structure and location of the underlying cold plasma in the plasmasphere, which has a strong influence on the efficiency of wave-particle interactions [Summers *et al.*, 2007]. The plasmaspheric outer boundary, known as the plasmopause [Carpenter, 1963], provides a line of demarcation between regions of high and low electron plasma frequency, but its location is highly variable dependent on geomagnetic activity levels [Carpenter and Anderson, 1992]. During geomagnetic storms the plasmopause can move from its nondisturbed $L \sim 5$ location to positions as low as $L \sim 2$ [O'Brien and Moldwin, 2003].

Cyclotron resonant wave-particle interactions respond differently to the differing electron gyrofrequency conditions due to plasma density changes either side of the plasmopause. VLF chorus waves dominate the interaction processes outside, plasmaspheric hiss dominates inside the plasmopause, and electron magnetic ion cyclotron waves appear most significant on the plasmopause [Summers *et al.*, 2007]. During large geomagnetic storms localized regions of the outer radiation belt can experience large changes in trapped flux levels, as well as wave-particle interaction processes that change as the storm evolves. These factors can make the attribution of the primary driving factors difficult to identify and the evolution of trapped and precipitated fluxes through a geomagnetic storm period hard to predict [Reeves *et al.*, 2003].

The influence of plasmaspheric hiss on electron precipitation in the $L = 3-4$ region has been assessed using pitch angle diffusion codes with wave power distributions based on satellite observations [see Meredith *et al.*,

2006a, and references therein]. Plasmaspheric hiss (<1 kHz) was found to be confined to the high-density plasmasphere, with wave amplitudes an order of magnitude higher on the dayside (06:00–18:00 magnetic local time (MLT)) than the nightside, particularly during geomagnetic storms [Meredith *et al.*, 2006b]. Meredith *et al.* [2006a] calculated that during geomagnetically active periods plasmaspheric hiss propagating at small-wave normal angles could influence electron precipitation rates from 100 to 2000 keV, over the L -shell range of $L=3$ –4. Meredith *et al.* [2006b] calculated that for electron precipitation energies of >500 keV loss time scales could be on the order of 1 day, while for 100–500 keV loss time scales were on the order of 10 days. At L shells less than $L=3$ the loss time scales were ~100 days or more for energies <1 MeV.

The electron precipitation spectrum driven by plasmaspheric hiss was inferred by Rodger *et al.* [2007] using data from the CRRES and DEMETER electron detectors and confirmed with ground-based narrowband radio wave observations. The spectrum of precipitating electrons was found to have an e -folding energy of 365 keV over the energy range of 100–2000 keV. Plasmaspheric hiss-induced daytime electron precipitation fluxes of $\sim 10^3$ el cm⁻² s⁻¹ sr⁻¹ > 150 keV were estimated at $L=3.2$ during the recovery phase of a large geomagnetic storm ($Dst \sim -120$ nT) in September 2005. The characteristics of electron precipitation due to plasmaspheric hiss between $L=3$ –4 were also investigated by Whittaker *et al.* [2014]. Using a superposed epoch analysis of electron precipitation observations made by the Polar Orbiting Environmental Satellite (POES) electron telescopes a >300 keV precipitating population was found with very little precipitation observed in the range of 30–300 keV. A study of a conjunction event between the Van Allen Probes and POES showed plasmaspheric hiss-driven electron precipitation >30 and >100 keV inside the plasmopause but also at $L > 4$ when the plasmopause was at $L > 5.8$ [Li *et al.*, 2014]. Peak plasmaspheric hiss wave power was observed at 100–200 Hz, which would undergo cyclotron resonance with electrons of ~100 keV at $L=4$ [Bortnik *et al.*, 2011].

When energetic electron precipitation enters the atmosphere it generates excess ionization at altitudes that are dependent on the electron energy [Turunen *et al.*, 2009]. The ionization increases generate odd nitrogen (NO_x) and odd hydrogen (HO_x) species. These species can catalytically destroy ozone with reaction efficiency dependent on altitude and solar photolysis conditions [Brasseur and Solomon, 2005]. The impact of electron precipitation has been observed, in terms of generating NO_x [Seppälä *et al.*, 2007], HO_x [Verronen *et al.*, 2011], and destroying ozone [Andersson *et al.*, 2014]. Ozone is an important constituent of the atmosphere, absorbing energy from the UV part of the solar spectrum and contributing to the radiation balance of the climate system [Brasseur and Solomon, 2005]. The introduction of increased levels of NO_x at ~80 km altitudes in coupled climate models has been shown to modify polar surface temperatures on seasonal time scales [Rozanov *et al.*, 2005]. The same surface geomagnetic activity-driven temperature modification was identified by Seppälä *et al.* [2009] using meteorological reanalysis data, and further modeling efforts confirmed the linkage between energetic particle precipitation and surface effects [Baumgaertner *et al.*, 2011]. The local time, geographic latitude, and longitude of energetic particle precipitation are important factors in the amount of chemical change caused in the atmosphere. Thus, the dynamics of the outer radiation belt and the underlying plasmasphere play an important role in determining the efficiency of the coupling between space weather effects and its atmospheric impact [Clilverd *et al.*, 2015].

In this study, we investigate the effects of a large geomagnetic storm that occurred on 25 October 2011, with particular focus on the impact of the dynamic plasmopause location. We analyze the observation of a large increase in trapped radiation belt flux at $L=3$ –4, probably as a result of whistler mode chorus-driven acceleration. This was then followed by a gradual decline to prestorm flux levels even though no significant precipitation fluxes could be observed in the POES electron precipitation detectors. We use the Antarctic-Arctic Radiation-belt (Dynamic) Deposition-VLF Atmospheric Research Konsortium (AARDDVARK) receiver network to investigate the characteristics of the electron precipitation throughout the storm period. We show that initial large electron precipitation fluxes at $L=3$ –4 during the nighttime are constrained to the storm main phase. Weaker, longer-lasting electron precipitation occurs on the dayside, probably driven by plasmaspheric hiss. The characteristics of each type of precipitation are determined, and we investigate if the observed precipitation into the atmosphere could account for the decay of the trapped fluxes after the storm.

2. Experimental Setup

To study the energetic electron precipitation fluxes into the atmosphere during the October–November 2011 period we use narrowband subionospheric very low frequency (VLF) data spanning 24–25 kHz

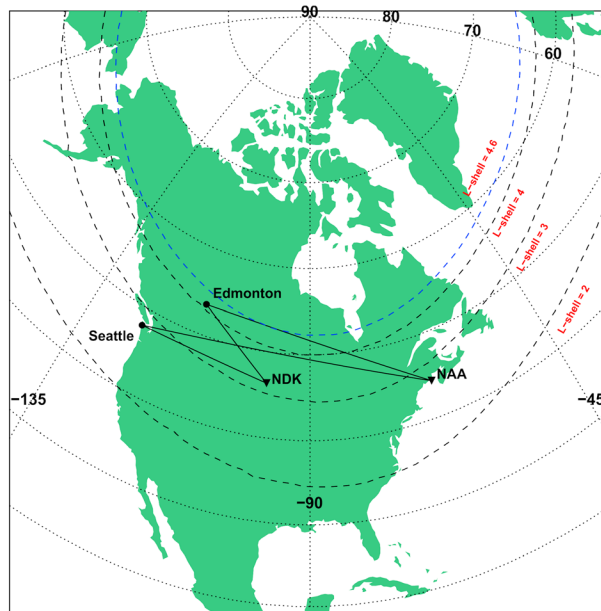


Figure 1. The subionospheric propagation paths from VLF transmitters NDK and NAA (triangles) to the AARDDVARK receiver site at Forks, Seattle, and Ministik Lake, Edmonton (circles). L -shell contours for $L = 2, 3$, and 4 are shown as black dashed lines, while an L -shell contour representing the quiet time location of the plasmopause at $L = 4.6$ is shown as a blue dashed line.

received at Forks, Seattle, Washington (geographic $47^{\circ}56'N$, $124^{\circ}24'W$; $L = 2.9$), and Ministik Lake, Edmonton, Canada (geographic $53^{\circ}21'N$, $112^{\circ}58'W$; $L = 4.0$). The Forks and Ministik sites are part of the AARDDVARK network (see *Clilverd et al.* [2009]; for further information see the description of the array at www.physics.otago.ac.nz/space/AARDDVARK_homepage.htm). The transmitters studied have call signs NAA (24.0 kHz; geographic $44^{\circ}39'N$, $67^{\circ}17'W$; $L = 2.9$) and NDK (25.2 kHz; geographic $46^{\circ}22'N$, $98^{\circ}20'W$; $L = 3.1$). Figure 1 shows the locations of the Forks, Seattle, and Ministik Lake, Edmonton, radio wave receiver sites (circles) and the transmitter-receiver paths that are studied during the event period (the NAA and NDK transmitter locations are shown by the triangles). Selected L -shell contours are also shown, with a typical location of the nondisturbed plasmopause given by the blue dashed line. The VLF propagation paths span the range of $3 < L < 4.6$,

effectively integrating the effects of subionospheric electron precipitation from the outer radiation belt inside of the plasmopause, particularly during nondisturbed conditions.

Figure 2 (top) shows the varying geomagnetic activity conditions during the 18 October to 14 November 2011 period that is studied in this paper. A large disturbance in the geomagnetic activity index, Dst , is seen to start on 24 October, quickly reaching values < -100 nT. Recovery from the geomagnetic storm continues from 25 to 30 October, with a smaller disturbance beginning on 1 November.

In this study we also make use of particle measurements by the Space Environment Monitor-2 instrument package on board the POES spacecraft as described in detail in *Simon Wedlund et al.* [2014]. The detectors pointing in the 0° and 90° directions are $\pm 15^{\circ}$ wide. Modeling has been used to determine the radiation belt populations monitored by the telescopes [*Rodger et al.*, 2010a, 2010b]. For the L shells that we consider the 90° detector appears to primarily respond to trapped electrons, although that does include a proportion of pitch angles that are only just above the loss cone, and hence, we will refer to it as the “quasi-trapped detector.” In contrast, the 0° detector views inside the bounce loss cone and provides a measurement of some fraction of the precipitating electron population. Hence, we will refer to it as the “precipitating detector.” It is widely accepted that the noise floor of the instrument is $100\text{--}200$ $\text{el cm}^{-2} \text{sr}^{-1} \text{s}^{-1}$ [*Neal et al.*, 2015], with some authors using values as high as 500 $\text{el cm}^{-2} \text{sr}^{-1} \text{s}^{-1}$ [*Li et al.*, 2014]. In addition, during periods of weak diffusion where the loss cone is not uniformly filled it has been found that POES may fail to detect some or all of the electrons close to the upper edge of the bounce loss cone fluxes which are precipitating into the atmosphere [*Hargreaves et al.*, 2010]. The fluxes of >30 keV electrons may need to be as high as 10^5 $\text{el cm}^{-2} \text{sr}^{-1} \text{s}^{-1}$ before the bounce loss cone is uniformly filled [*Rodger et al.*, 2013].

In Figure 2 we also show the >100 keV POES quasi-trapped (Figure 2, middle) and precipitating (Figure 2, bottom) electron fluxes as a function of L shell during the study period. The format of this type of plot is described in detail by *Simon Wedlund et al.* [2014]. Several enhancements in flux can be seen in the quasi-trapped fluxes, particularly on 24 October 2011 and again on 1 November. The precipitating fluxes also increase on these dates. A modeled plasmopause location using the Kp -driven O’Brien and Moldwin plasmopause model [*O’Brien and Moldwin*, 2003] is plotted on both panels and indicates that the majority of the electron precipitation takes place outside of the plasmopause. Significant quasi-trapped electron fluxes

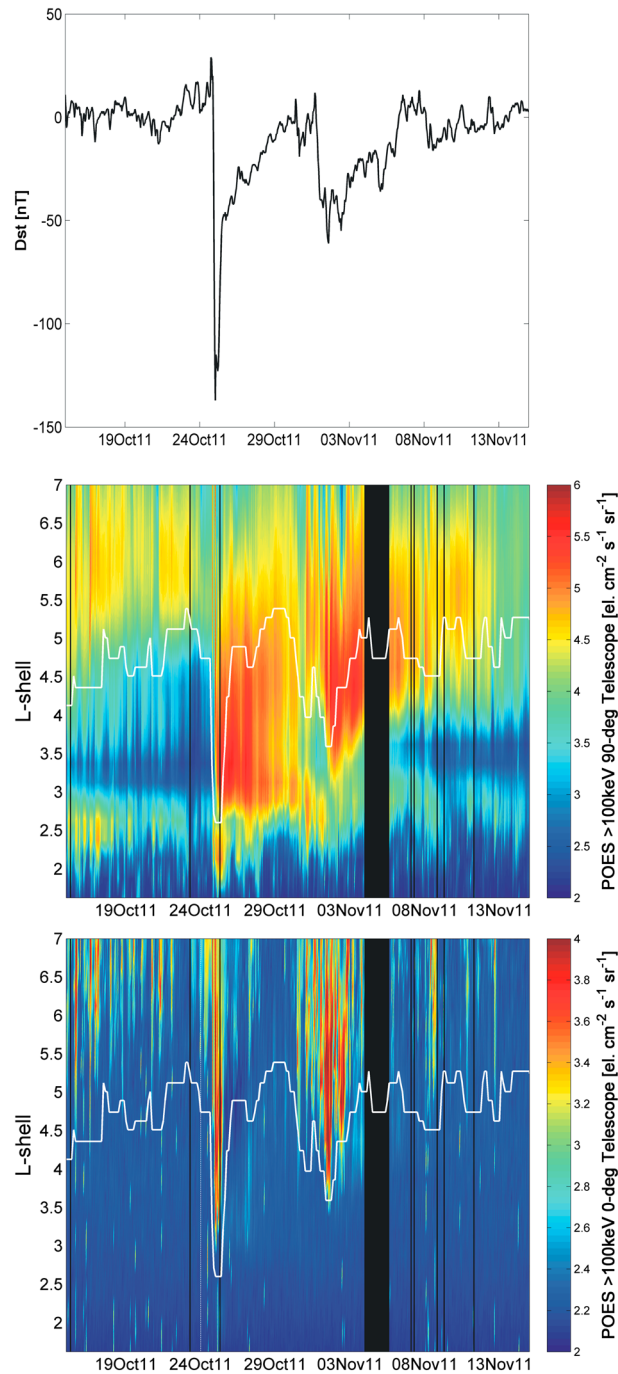


Figure 2. (top) The variation of the geomagnetic activity index, *Dst*, during 18 October to 14 November 2011. A geomagnetic disturbance begins on 24 October 2011, with recovery conditions occurring until 1 November. The zonally averaged >100 keV POES (middle) quasi-trapped and (bottom) precipitating electron fluxes during the study period in October–November 2011. The *L*-shell ranges cover the inner and outer radiation belts, where several enhancements in flux can be seen. The color scales represent \log_{10} of electron flux ($\text{cm}^{-2} \text{s}^{-1} \text{sr}^{-1}$), with black representing missing data. A model of the location of the plasmapause is shown as a white line in both panels.

are observed inside of the plasmapause ($L = 3\text{--}4.5$) following the geomagnetic disturbance on 24 October, with flux levels gradually decreasing toward the end of October. However, no resulting increase in precipitation into the atmosphere is observed by POES in that time period. The quasi-trapped >30 keV fluxes declined by about 1 order of magnitude during the 6 day recovery period after the storm on 24 October, until being interrupted by another geomagnetic disturbance. The quasi-trapped >100 and >300 keV fluxes also declined during the 6 day period but showed signs of initial increases for the first few days.

3. Results

Subionospheric radio waves observed by the AARDDVARK network propagate from a transmitter to a receiver. Any electron precipitation occurring along the great circle path from transmitter to receiver will cause changes in the received amplitude of the radio waves if the energy of the electron is such that excess ionization is created at or below the lower edge of the *D* region ionosphere. Figure 3 (top row) shows the amplitude variation of the NAA and NDK transmitters received at Forks, Seattle. The amplitude data are presented with 0.5 h resolution, and the color scales represent voltage relative to an arbitrary level (in decibel). The *x* axis shows universal time, while the *y* axis displays the dates from 18 October 2011 to 05 November 2011. NAA-Forks, Seattle, is displayed on the left-hand side. The *L*-shell range of the propagation path is $L = 2.9\text{--}4.0$ (see Figure 1). NDK-Forks, Seattle, is on the right, and the *L*-shell range of the propagation path is $L = 2.9\text{--}3.1$, well within the plasmapause apart from during the most intense phase of the storm (see Figure 2). A horizontal white line indicates the day of the geomagnetic storm onset as shown in Figure 2. Daytime ionospheric propagation conditions are observed from 14:00 to 22:00 UT, and nighttime

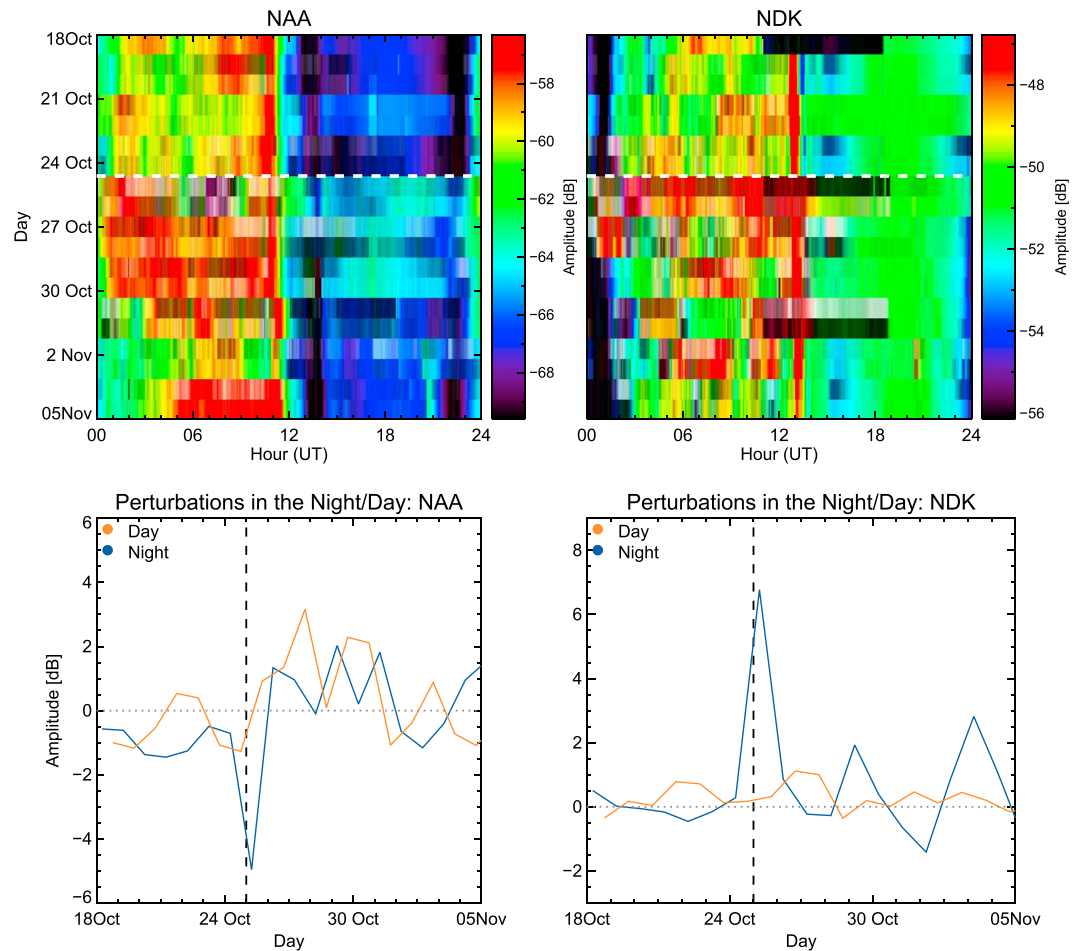


Figure 3. (top row) Median amplitude variations of the NAA and NDK transmitters received at Forks, Seattle, from 18 October to 05 November 2011. The color scale is in decibel relative to an arbitrary voltage. A horizontal white dashed line represents the storm onset time on 24 October 2011. (bottom row) NAA and NDK amplitude perturbations during the study period. Perturbations are calculated from nondisturbed values. Daytime (19:30 UT, red line) and nighttime (06:00 UT, blue line) lines are shown. The vertical black dashed lines represent the storm onset time on 24 October 2011.

conditions occur from 02:00 to 10:00 UT. The three periods of low amplitude (e.g., 11:00–19:00 UT on NDK) are the weekly off-air periods that the transmitters undergo. In the NAA-Seattle panel a clear decrease in amplitude is observed during the night immediately following the start of the storm, with a further period of increased amplitudes following immediately afterward. During the daytime the amplitudes are observed to increase (from blue to green) a day or so after the start of the storm, remaining elevated until about 30 October. The NDK-Seattle amplitude variation is similarly elevated during the daytime after the storm but is also elevated at night at the start of the storm, opposite to the behavior seen in NAA-Seattle.

Figure 3 (bottom row) shows time slices of amplitude perturbation relative to nondisturbed levels at 06:00 UT and 19:00 UT, blue representing night and orange representing daytime propagation conditions on the paths (equivalent to 22:00–23:00 MLT and 11:00–12:00 MLT, respectively). The nondisturbed levels are obtained by averaging the amplitude measurements during quiet periods at the specified local times. The time slices clearly show the large nighttime perturbations at the peak of the geomagnetic storm indicated by the vertical dashed line. Small positive perturbations in daytime amplitudes can be observed, particularly for NAA-Seattle, lasting 6 days after the main phase of the storm. The lack of any significant daytime response in the NDK-Seattle path is likely to be due to the low L shell of the path ($L = 2.9\text{--}3.1$) being close to the inner edge of the precipitation region.

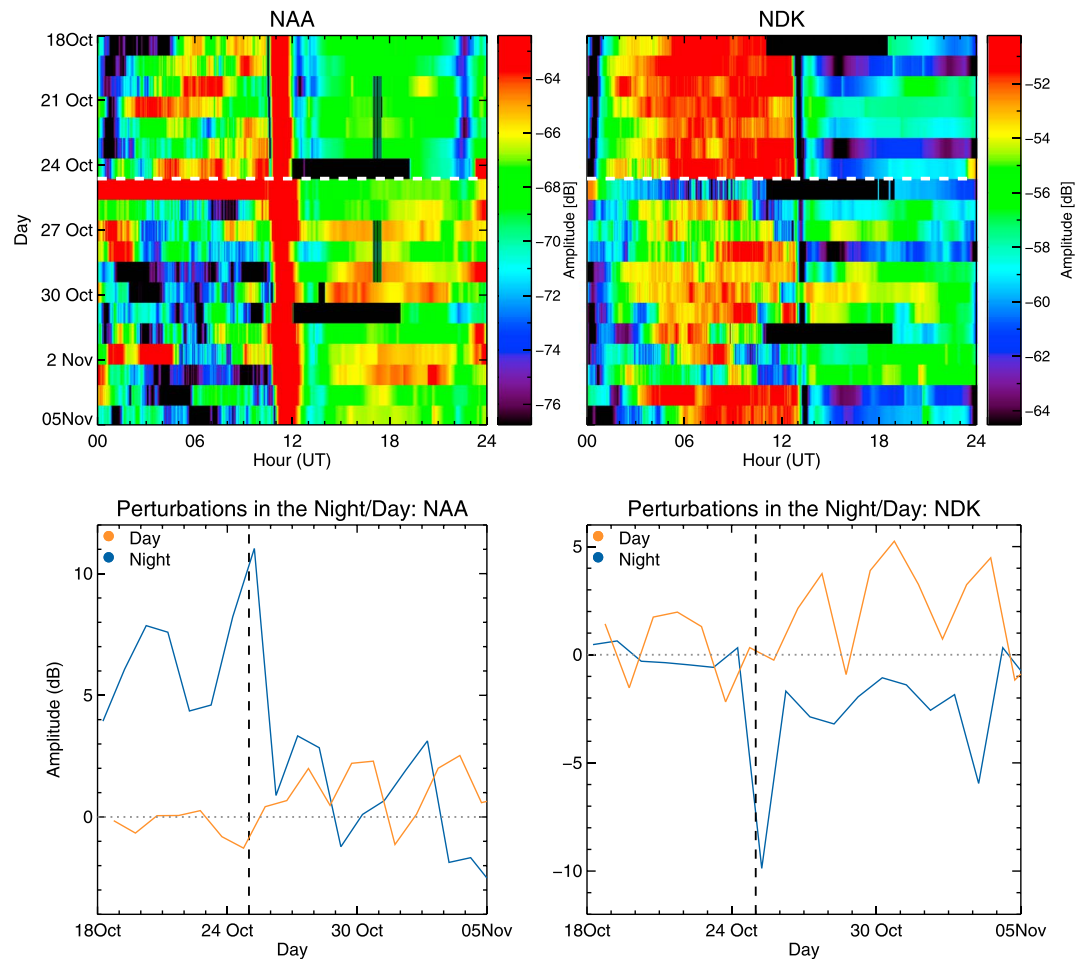


Figure 4. Same as in Figure 3 but for the NAA and NDK transmitters received at Ministik Lake, Edmonton.

Figure 4 is a similar format as Figure 3, although in this case the propagation paths are NAA and NDK received at Ministik Lake, Edmonton. The L -shell ranges of the propagation paths are $L = 3.1\text{--}4.0$ for NDK-Edmonton, while for NAA-Edmonton are $L = 2.9\text{--}4.6$, and this represents a path that passes close to the footprint of the nondisturbed plasmapause. Once again, poststorm increases in amplitude can be observed during the day, typically lasting 6 days or so until the end of October. At night NAA-Edmonton exhibits a large positive perturbation during the main phase of the storm, and NDK-Edmonton shows a large negative perturbation.

The main features exhibited by the four transmitter-receiver paths shown here suggest two outstanding characteristics. At night, around 00:00 MLT, there are strong disturbances coincident with the main phase of the storm on 25 October. This is consistent with the inward movement of the plasmapause to lower L shells during the geomagnetic storm and the impact of electron precipitation from outside of the plasmapause on the propagation paths as suggested by Figure 2. During the day, around 12:00 MLT, there are perturbations observed after the main phase of the storm, lasting for 5 or more days. During this period the plasmapause is likely to be significantly poleward of the $L = 2.9\text{--}4.6$ propagation paths as suggested by Figure 2, and dayside precipitation from inside of the plasmasphere is causing the observed perturbations.

4. Electron Precipitation Flux From NDK and NAA Observations

The VLF wave propagation of NDK and NAA to either Seattle or Edmonton is calculated using the Long Wave Propagation Code (LWPC) [Ferguson and Snyder, 1990], which models VLF signal propagation from any point on Earth to any other point as described in detail by Simon Wedlund et al. [2014]. To model the perturbation

we assume that the whole path is affected by excess ionization which is superimposed on the underlying “ambient” ionosphere. This process has been described most recently in *Rodger et al.* [2013] and *Simon Wedlund et al.* [2014] and will only be very briefly summarized here. The sharpness parameter β and a reference height h' [Wait and Spies, 1964] of the nondisturbed ionospheric profiles are given by *McRae and Thomson* [2000], or *Thomson and McRae* [2009], or *Thomson et al.* [2011], depending on the local time being modeled. An excess ionization rate is calculated from the precipitating energetic electrons which have a spectral gradient varying with a power law scaling exponent (k). The electron number density profiles determined for varying precipitation flux magnitudes and varying k are used as input to the LWPC subionospheric propagation model.

4.1. Modeling the Nighttime Perturbations

The nighttime perturbations on the $L=2.9$ – 4.6 propagation paths studied here are primarily caused by electron precipitation from outside of the plasmapause most likely driven by chorus waves [Horne, 2002]. In this study the chorus-driven electron precipitation only affects the four propagation paths during the most intense period of the geomagnetic storm, when the plasmapause is pushed inward to $L < 3$. In Figure 2 the >100 keV electron POES precipitating fluxes between $L=3$ – 4.5 during the night of 25 October 2011 are $\sim 5 \times 10^3$ el cm $^{-2}$ sr $^{-1}$ s $^{-1}$, with similarly high fluxes observed in the >30 and >300 keV detectors. High precipitating flux levels observed by POES during large geomagnetic storms are consistent with strong scattering conditions and a near-uniform distribution of flux across the loss cone pitch angle range [Hargreaves et al., 2010; Rodger et al., 2013; Simon Wedlund et al., 2014; Neal et al., 2015]. Thus, we can use the POES >30 , >100 , and >300 keV measurements to accurately determine the energy spectrum of the precipitating electrons. During the period of 00:00–09:00 UT on 25 October 2011, and over the L -shell range of $L=3.0$ – 4.5 , the power law spectral gradient (k) was -3 . This is in good agreement with the spectral gradient of electron precipitation generated by chorus during high geomagnetic activity conditions determined by *Simon Wedlund et al.* [2014]. The $k=-3$ power law spectral gradient was used to calculate the perturbation effect on each radio wave propagation path using this spectrum and over a range of flux values. The spectral range was limited to 10–3000 keV and the flux magnitude range to 10^{-1} – 10^6 el cm $^{-2}$ sr $^{-1}$ s $^{-1}$ for >30 keV electrons. The ambient ionosphere in this case was given by a previously reported nighttime profile [Thomson et al., 2007].

Figure 5 shows the amplitude perturbations as a function of chorus-induced flux magnitude for each transmitter-receiver path. The lowest average L -shell path (NDK-Seattle, $L=2.9$ – 3.1) is shown in Figure 5, top left, while the highest average L -shell path (NAA-Edmonton, $L=2.9$ – 4.6) is shown in Figure 5, bottom right. The lowest L shell of any of the propagation paths is $L=2.9$ which, as shown in Figure 2 (bottom), is close to the L shell of the calculated plasmapause location at the peak of the geomagnetic storm. Thus, we can reasonably assume that chorus-driven precipitation outside of the plasmasphere is acting over the whole of the propagation paths discussed here. Dependent on path, the amplitude perturbations vary from positive or negative changes and can be either big or small. For the two midrange paths (NAA-Seattle and NDK-Edmonton), the observed perturbations of -5 dB and -10 dB, respectively, indicate that >30 keV fluxes of $\sim 10^4$ el cm $^{-2}$ sr $^{-1}$ s $^{-1}$ are involved over the range of $L=3$ – 4 . On the $L \sim 3$ path (NDK-Seattle), the observed perturbation of $+6$ dB is not reproduced in the modeling using a $k=-3$ spectrum but would be possible if the spectrum was softer, i.e., $k \sim -4$ with a >30 keV flux magnitude of $\sim 10^3$ el cm $^{-2}$ sr $^{-1}$ s $^{-1}$. Modeling of the highest average L -shell path (NAA-Edmonton) results in negative perturbations for most imposed fluxes. However, the observations suggest a $+10$ dB perturbation effect. At present we are unable to model the observed NAA-Edmonton nighttime amplitude perturbation on this path even when other spectral gradient values are investigated. The cause of this difficulty in modeling the NAA-Edmonton path is probably due to uncertainties in the LWPC surface conductivity values as the propagation path crosses the wet, peaty soil of the region to the south of the Hudson Bay. This causes extra mode conversion (because the ground is not uniform over distances as small as tens of kilometer); this additional mode conversion will likely be more significant at night because so many more modes survive over significant distances at night as compared with day (N. R. Thomson, personal communication, 2015). However, the results from the three other paths suggest that >30 keV electron fluxes with magnitude $\sim 10^4$ el cm $^{-2}$ sr $^{-1}$ s $^{-1}$ are precipitated into the atmosphere at $L=3$ – 4 during the main phase of the geomagnetic storm on 25 October 2011. These findings are in agreement with the observed zonally

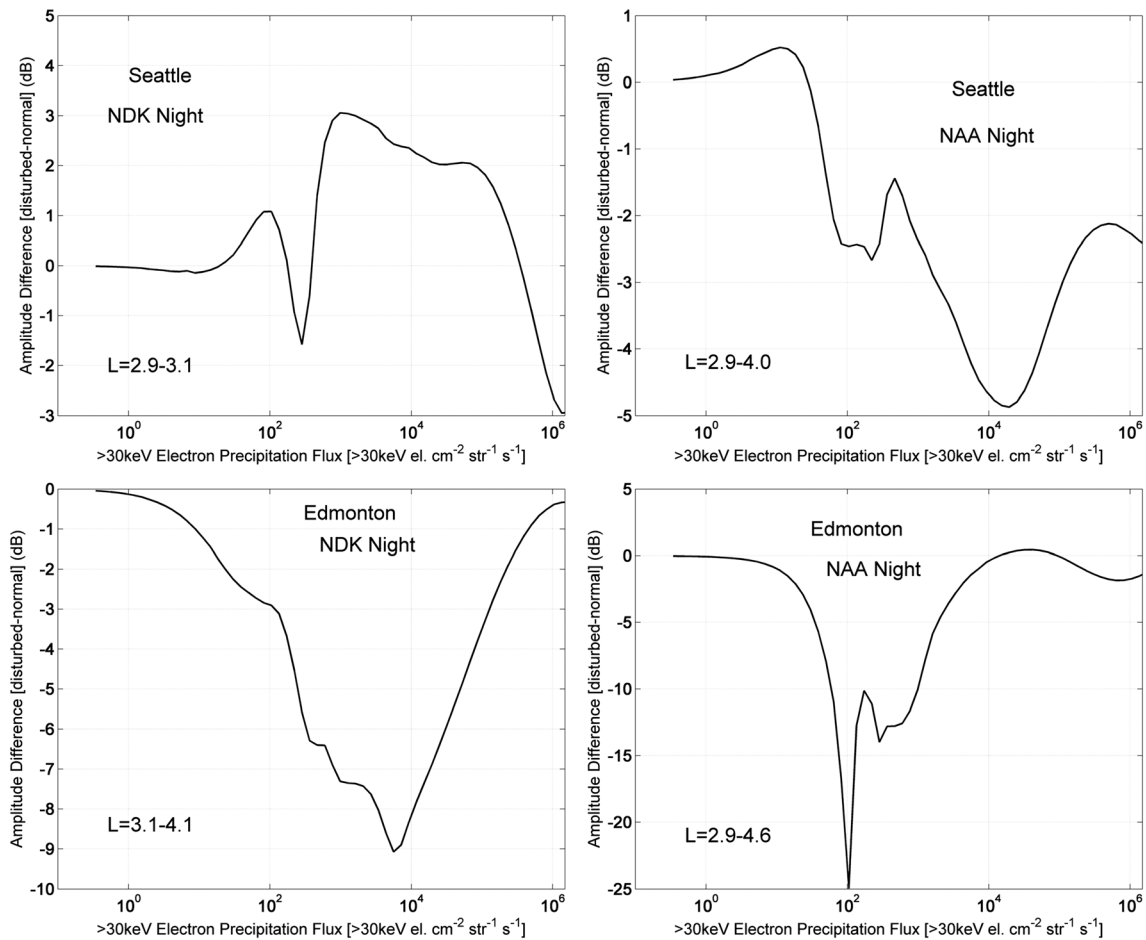


Figure 5. Modeled night perturbations in (top left) NDK amplitude and (top right) NAA amplitude at Forks, Seattle, for varying magnitudes of >30 keV electron precipitation flux. Modeled night perturbations in (bottom left) NDK amplitude and (bottom right) NAA amplitude at Ministik Lake, Edmonton, for varying magnitudes of >30 keV electron precipitation flux. The electron precipitation is modeled with a 10 – 3000 keV energy spectrum with a -3 power law gradient consistent with chorus-induced electron precipitation [Whittaker *et al.*, 2014]. The L -shell ranges of the propagation paths are indicated on each plot.

averaged fluxes reported by POES in the same L -shell range, consistent with strong chorus-driven wave-particle diffusion conditions uniformly filling the loss cone. At the lower edge of the study region provided by the various propagation paths ($L \sim 3$), the fluxes are found to be lower and the spectral gradient is steeper, although this is not observed by POES as the >100 and >300 precipitation fluxes are affected by the instrument sensitivity limit.

4.2. Modeling the Daytime Perturbations

The daytime perturbations on the $L = 2.9$ – 4.6 propagation paths studied here are primarily caused by electron precipitation from inside of the plasmapause most likely driven by plasmaspheric hiss waves [Smith *et al.*, 1974]. We have inspected Cluster spacecraft data using the STAFF-SA and Waves of High frequency and Sounder for Probing of Electron density by Relaxation instruments [Santolik *et al.*, 2006] during the period following the geomagnetic storm on 25 October 2011. Plasmaspheric hiss was observed on 26, 28, and 30 October, primarily on the dayside (07:00–15:00 MLT), and at $L < 3.7$. Thus, the Cluster spacecraft observations are consistent with the idea that plasmaspheric hiss is present within the dayside plasmasphere and could be taking part in wave-particle interactions that drive electron precipitation following the geomagnetic storm. In order to be able to model the response of the four transmitter-receiver paths studied here a characteristic spectrum needs to be applied. Dayside electron precipitation at $L \sim 3$ driven by plasmaspheric hiss was investigated by Rodger *et al.* [2007] using DEMETER and CRRES

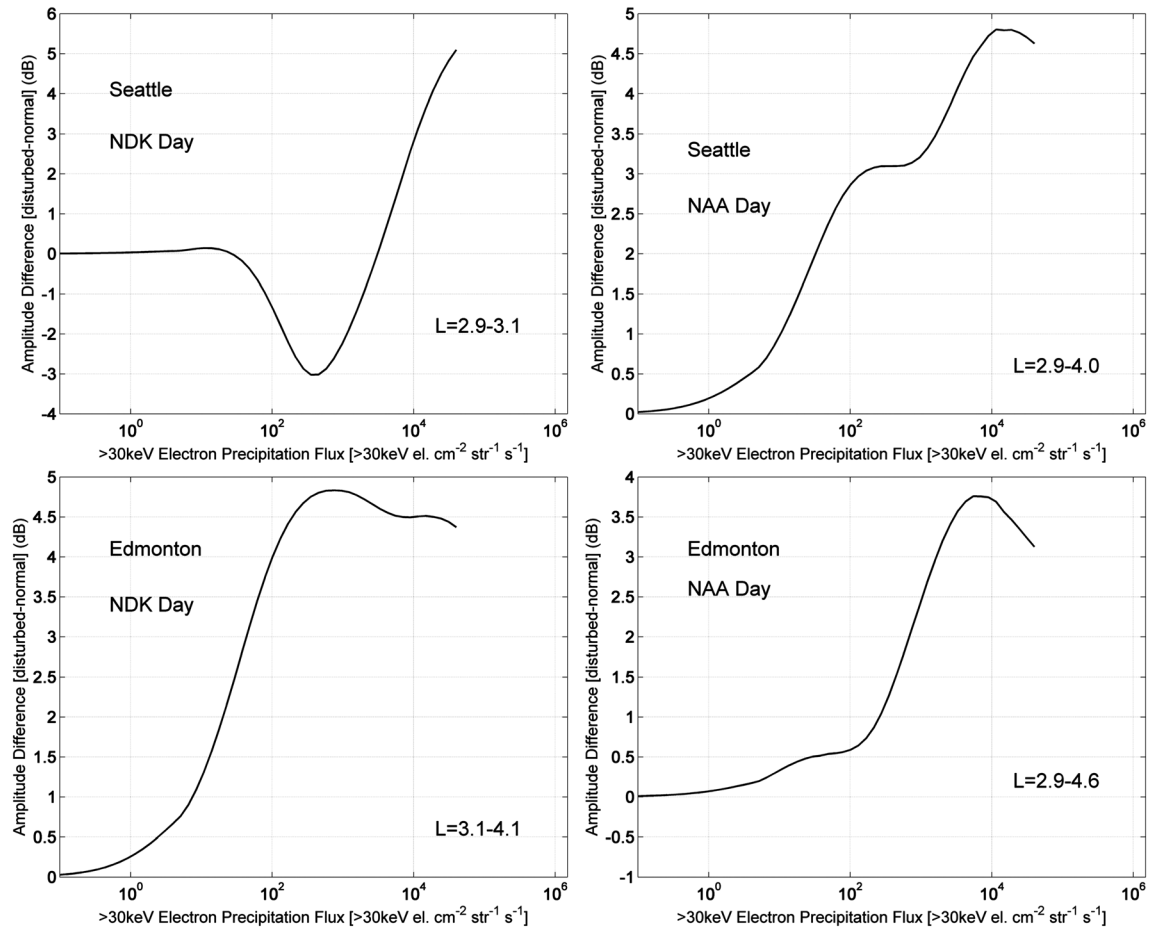


Figure 6. Same as in Figure 5. However, in this case the electron precipitation is modeled with a 365 keV *e*-folding spectrum consistent with plasmaspheric hiss-induced electron precipitation [Rodger *et al.*, 1998], and the radio wave propagation conditions are for a daytime ionosphere.

satellite data, confirming the observations with ground-based AARDDVARK data. The electron precipitation spectrum observed was a 365 keV *e*-folding type. Here we calculate the perturbation effect on each radio wave propagation path using this spectrum and over a range of flux values. As before, the spectral range was limited to 10–3000 keV and the >30 keV flux magnitude range to 10⁻¹–10⁶ el cm⁻² sr⁻¹ s⁻¹. The ambient ionosphere is specified using daytime ionospheric parameters to describe the conditions along the path [Thomson *et al.*, 2011].

Figure 6 shows the variation in amplitude for all four paths as the precipitation flux is varied. Typically, the amplitude perturbation is positive and increases with increasing flux. In section 3 we showed that daytime perturbation values were ~2–3 dB for the NAA-Seattle path (*L* = 2.9–4.0), which this modeling shows is indicative of >30 keV flux magnitude values of ~10² el cm⁻² sr⁻¹ s⁻¹. This is close to the sensitivity limit of POES and would explain why no precipitating fluxes could be observed by the satellite detectors. The calculated fluxes were highest on 27 October and 29–30 October. The NDK-Edmonton path covering a similar *L*-shell range (*L* = 3.1–4.1) showed daytime perturbations of 3–5 dB, which also correspond to >30 keV flux magnitudes of ~10² el cm⁻² sr⁻¹ s⁻¹, and the calculated fluxes were also highest on 27 and 29–30 October. The lowest *L*-shell path studied, NDK-Seattle (*L* = 2.9–3.1), showed only small perturbation amplitudes and for only a few days. On 26 and 27 October perturbations of ~1 dB suggest >30 keV flux magnitudes of ~10⁴ el cm⁻² sr⁻¹ s⁻¹, with very low level fluxes of <10¹ el cm⁻² sr⁻¹ s⁻¹ for the remainder of the study period. The highest *L*-shell path studied, NAA-Edmonton (*L* = 2.9–4.6), showed perturbations of ~2 dB corresponding to >30 keV flux magnitudes of ~10³ el cm⁻² sr⁻¹ s⁻¹, peaking on 27 and 29–30 October as with the other paths.

Three of the paths studied are consistent in the indication of low levels of dayside precipitation flux from inside of the plasmopause ($L \sim 3\text{--}4.5$) lasting from 25 to 30 October. The lowest L -shell path at $L \sim 3$ shows only a brief period of precipitation lasting until 27 October, with the accurate identification of flux levels present made uncertain by the small perturbation values exhibited. This suggests that $L = 3$ is close to the inner edge of the plasmaspheric hiss-induced precipitation region; this is consistent with the findings of Whittaker *et al.* [2014] using superposed POES observations. In the L -shell range of $L \sim 3\text{--}4.5 > 30$ keV flux magnitudes peak at $\sim 10^2 \text{ el cm}^{-2} \text{ sr}^{-1} \text{ s}^{-1}$, which is close to the sensitivity limit of the POES electron detectors and potentially explains the lack of observed precipitation by POES.

We have shown that the observed $L = 3\text{--}4.5$ radio wave perturbations during, and after, a geomagnetic disturbance can be reasonably modeled in order to provide electron precipitation fluxes. The >30 keV precipitation fluxes during the main phase of the geomagnetic storm appear to be driven by chorus waves located outside of the plasmopause. The determined fluxes are consistent with the levels measured by POES at the time, and those described by Whittaker *et al.* [2014] in a superposed epoch study of geomagnetic storms, i.e., >30 keV electron flux of $\sim 10^4 \text{ el cm}^{-2} \text{ sr}^{-1} \text{ s}^{-1}$. The $L = 3\text{--}4.5 > 30$ keV precipitation fluxes during the recovery phase of the storm can be reasonably modeled by an e -folding energy spectrum consistent with that previously associated with plasmaspheric hiss. The L -shell range of the precipitation and the observation of precipitation fluxes primarily on the dayside are also suggestive of the involvement of plasmaspheric hiss in the recovery phase of the storm.

5. The Loss of Trapped Fluxes Within the Plasmasphere

Immediately following the geomagnetic storm in October 2011 enhanced >30 , >100 , and >300 keV quasi-trapped electron fluxes were observed inside of the plasmopause at $L = 3\text{--}4.5$. After the storm the quasi-trapped fluxes slowly recovered toward their initial levels over a period of 5–7 days. However, no enhanced electron precipitation fluxes were observed inside of the plasmopause by the POES >30 , >100 , and >300 keV telescopes at this time. Nevertheless, detectable changes in radio wave propagation conditions were observed on daytime paths that crossed under the magnetic field-line footprints of the plasmasphere at $L = 3\text{--}4.5$. By using an electron precipitation energy spectrum published for plasmaspheric hiss ($E_0 = 365$ keV [Rodger *et al.*, 2007]), we have been able to reasonably model the perturbations of the radio wave propagation conditions, finding that >30 keV fluxes of $\sim 100 \text{ el cm}^{-2} \text{ s}^{-1} \text{ sr}^{-1}$ were occurring and lasting for 5–7 days. These flux levels are close to the sensitivity limit of the POES electron detectors ($\sim 100 \text{ el cm}^{-2} \text{ s}^{-1} \text{ sr}^{-1}$) and would explain the lack of enhanced precipitation fluxes in the SEM-2 telescopes.

We wish to test whether such low precipitation fluxes, with magnitudes near the POES noise floor level, are able to deplete the trapped radiation belt population on time scales similar to that observed by POES after the 24 October 2011 storm. To do this we calculate the total population of electrons in a flux tube, integrated with energy and normalized to the trapped values reported by the POES 90° detector. This population is then depleted at a steady rate consistent with the AARDDVARK- and POES-determined precipitation fluxes to find the decay rate expected in the trapped fluxes, assuming that this is the dominant loss process. This is a fairly common approach used in experimental studies to determine the overall significance of precipitation to the radiation belts [e.g., Voss *et al.*, 1998; Lorentzen *et al.*, 2001; Rodger *et al.*, 2003; O'Brien *et al.*, 2004; Blum *et al.*, 2013].

Using the assumed e -folding precipitation spectrum of $E_0 = 365$ keV, combined with the inferred >30 keV precipitation flux levels of $100 \text{ el cm}^{-2} \text{ s}^{-1} \text{ sr}^{-1}$, we calculate the rate of decay of the trapped fluxes in a theoretical POES 90° detector, assuming a $n = 2.5$ dependence of the fluxes to pitch angle following Blum *et al.* [2013] and taking the approach to calculate flux tube populations given in section 5 of Rodger *et al.* [2003]. Figure 7 shows the effect of depleting trapped fluxes in the >30 , >100 , and >300 keV ranges for 5 days (modeled values indicated by solid lines, observations indicated by dashed lines). The calculation was made to represent the pitch angles of the POES 90° telescopes, starting from levels that were seen after the main phase of the geomagnetic storm. We assume that the precipitating flux is active for 24 h each day. If, as is more likely, the precipitation is only occurring for 12 h in each day (equivalent to 06:00–18:00 MLT), the effects shown are equivalent to a precipitation flux of $200 \text{ el cm}^{-2} \text{ s}^{-1} \text{ sr}^{-1}$ for >30 keV electrons. Day 0 represents 26 October 2011. We assume that calculated fluxes will reflect those of the trapped fluxes at POES altitudes (equivalent to an equatorial pitch angle of about 8°). As a result of

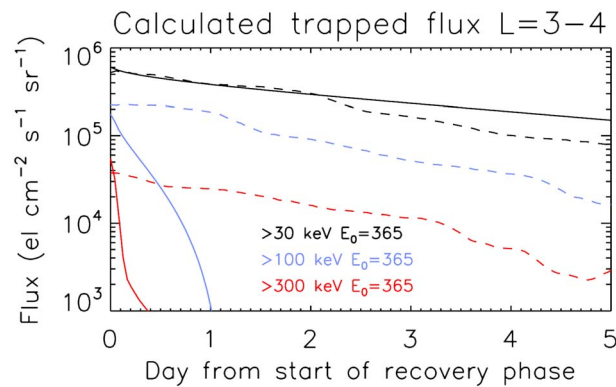


Figure 7. Calculated evolution of the POES 90° fluxes at >30 keV (black lines), >100 keV (blue lines), and >300 keV (red lines) caused by precipitation driven by plasmaspheric hiss with parameters described in the text (solid lines). The dashed lines indicate the observed POES quasi-trapped electron flux variation from the start of the recovery phase of the 25 October 2011 geomagnetic storm.

the imposed loss from precipitation into the atmosphere the calculated >30 keV trapped fluxes are reduced by about an order of magnitude in 5 days. The >100 keV fluxes are reduced by 2 orders of magnitude in ~1 day and the >300 keV fluxes by the same amount in about half a day. This behavior is in agreement with those values estimated by Meredith *et al.* [2006b], where loss rates increased with increasing energy.

The observed POES 90° electron fluxes following the storm on 25 October are indicated by the dashed lines. Comparison between the calculated flux variation and the observations suggests that >30 keV fluxes are lost at a rate that is roughly consistent with the observed rate. However, the >100 keV and >300 keV trapped fluxes decrease more quickly than is observed, whereas the electron loss time scales between 100 and 300 keV in Meredith *et al.* [2006b] are in the order of days and are reasonably consistent with these observations. Overall, these results suggest that an electron precipitation spectrum with $E_0 = 365$ keV, from plasmaspheric hiss, has the capability to drive the observed decay of the trapped fluxes in POES measurements even while the fluxes are too low for the POES precipitation telescopes to register that any precipitation is occurring. However, the observed decay times are essentially the same at all three of the energy ranges while in a system where only plasmaspheric hiss losses are occurring, we estimate that the higher-energy electrons should be lost faster than the low-energy populations when the precipitation spectrum has $E_0 = 365$ keV, as we have shown. It is possible that as well as scattering into the loss cone taking place, there is also some in situ acceleration of the electrons, counteracting on the decay of the fluxes of the >100 and >300 keV channels. This is consistent with the idea that trapped electron flux variation is due to “a delicate balance between acceleration and loss” [Reeves *et al.*, 2003]. Our results may suggest that the plasmaspheric hiss waves are taking part in wave-particle amplification processes in the plasmasphere at these higher energies or that there could be an additional source provided by radial transport [Li and Temerin, 2001]. We note that it is very challenging to accurately estimate the total flux tube population and their evolution with time on the basis of observations from low Earth orbit. In particular, the assumed pitch angle distribution is a quite sensitive parameter when calculating the decay times.

6. Summary

We find that during a large geomagnetic storm in October 2011 the quasi-trapped fluxes of >30, >100, and >300 keV radiation belt electrons are enhanced at $L = 3-4$ during the main phase. This is initially due to chorus-driven wave-particle acceleration occurring when the plasmopause was located at $L < 3$ for ~9 h. During the storm recovery phase the plasmopause returned to typical nondisturbed L shells ($L \sim 4.5$), and the quasi-trapped fluxes at $L = 3-4$ slowly declined over 6 days. However, no electron precipitation into the atmosphere was detected by the POES >30, >100, and >300 keV 0° loss cone telescopes during the decay of the quasi-trapped fluxes. Conversely, the AARDDVARK network of radio wave receivers did detect dayside changes in radio wave propagation on paths that respond to electron precipitation from $L = 3-4$. The perturbation levels were found to be caused by >30 keV precipitation fluxes with magnitude $\sim 100 \text{ el cm}^{-2} \text{ s}^{-1} \text{ sr}^{-1}$ using a previously published plasmaspheric hiss-induced electron energy e -folding spectrum of $E_0 = 365$ keV [Rodger *et al.*, 2007]. The low levels of precipitation explain the lack of response of the POES telescopes to the flux. The detection of dayside, inner plasmasphere electron precipitation during the recovery phase of the storm is consistent with plasmaspheric hiss wave-particle interactions.

Estimates of the loss time scales due to the plasmaspheric hiss using the electron precipitation characteristics found in this study suggest time scales of days at >30 keV but hours at >100 keV and >300 keV. The calculations agree with observed loss time scales for >30 keV quasi-trapped fluxes observed by the POES 90° detectors but are much shorter than observed at >100 and >300 keV. These results suggest that plasmaspheric hiss has the capability to drive the observed decay rates of the trapped fluxes. It is possible that acceleration of the >100 and >300 keV fluxes inside of the plasmasphere was also taking place at the same time as losses into the atmosphere were occurring, counteracting the effects of pitch angle scattering into the loss cone. Further modeling work is needed in order clarify the processes behind these observations.

Acknowledgments

The observations obtained, and research leading to these results, has received funding from the European Union Seventh Framework Programme (FP7/2007-2013) under PLASMON grant agreement 263218. R.H.H. also acknowledges the PLASMON grant 263218 to the University of Washington. Data for this paper are available at the British Antarctic Survey Polar Data Centre (<http://psddb.nerc-bas.ac.uk/data/access/>). C.J.R. was partly supported by the New Zealand Marsden Fund. M.A.C., R.L.H., and R.D. would also like to acknowledge NERC funding as part of the Space Weather and Atmosphere Programme at the British Antarctic Survey.

M. Balikhin thanks the reviewers for their assistance in evaluating this paper.

References

- Andersson, M., P. T. Verronen, C. J. Rodger, M. A. Clilverd, and A. Seppälä (2014), Missing driver in the Sun–Earth connection from energetic electron precipitation impacts mesospheric ozone, *Nat. Commun.*, *5*, doi:10.1038/ncomms6197.
- Baumgaertner, A. J. G., A. Seppälä, P. Jöckel, and M. A. Clilverd (2011), Geomagnetic activity related NO_x enhancements and polar surface air temperature variability in a chemistry climate model: Modulation of the NAM index, *Atmos. Chem. Phys.*, *11*, 4521–4531, doi:10.5194/acp-11-4521-2011.
- Blum, L. W., Q. Schiller, X. Li, R. Millan, A. Halford, and L. Woodger (2013), New conjunctive CubeSat and balloon measurements to quantify rapid energetic electron precipitation, *Geophys. Res. Lett.*, *40*, 5833–5837, doi:10.1002/2013GL058546.
- Bortnik, J., L. Chen, W. Li, R. M. Thorne, N. P. Meredith, and R. B. Horne (2011), Modeling the wave power distribution and characteristics of plasmaspheric hiss, *J. Geophys. Res.*, *116*, A12209, doi:10.1029/2011JA016862.
- Brasseur, G. P., and S. Solomon (2005), *Aeronomy of the Middle Atmosphere: Chemistry and Physics of the Stratosphere and Mesosphere*, *Atmospheric and Oceanographic Sciences Library*, vol. 32, 3rd ed., p. 646, Springer, Netherlands.
- Carpenter, D. L. (1963), Whistler evidence of a “knee” in the magnetospheric ionization density profile, *J. Geophys. Res.*, *68*, 1675–1682, doi:10.1029/JZ068i006p01675.
- Carpenter, D. L., and R. R. Anderson (1992), An ISEE/whistler model of equatorial electron density in the magnetosphere, *J. Geophys. Res.*, *97*, 1097–1108, doi:10.1029/91JA01548.
- Clilverd, M. A., et al. (2009), Remote sensing space weather events: The AARDDVARK network, *Space Weather*, *7*, S04001, doi:10.1029/2008SW000412.
- Clilverd, M. A., C. J. Rodger, M. Andersson, P. T. Verronen, and A. Seppälä (2015), Linkages between the radiation belts, polar atmosphere and climate: Electron precipitation through wave particle interactions, in *Waves, Particles and Storms in Geospace*, edited by I. Mann et al., Oxford Univ. Press, Oxford.
- Ferguson, J. A., and F. P. Snyder (1990), *Computer Programs for Assessment of Long Wavelength Radio Communications*, Tech. Doc. 1773, p. 57, Natl. Ocean Syst. Cent., San Diego, Calif.
- Hargreaves, J. K., M. J. Birch, and D. S. Evans (2010), On the fine structure of medium energy electron fluxes in the auroral zone and related effects in the ionospheric D-region, *Ann. Geophys.*, *28*, 1107–1120, doi:10.5194/angeo-28-1107-2010.
- Horne, R. B. (2002), The contribution of wave particle interactions to electron loss and acceleration in the Earth’s radiation belts during geomagnetic storms, in *Review of Radio Science 1999–2002*, edited by W. R. Stone, chap. 33, pp. 801–828, John Wiley, New York.
- Li, W., et al. (2014), Quantifying hiss-driven energetic electron precipitation: A detailed conjunction event analysis, *Geophys. Res. Lett.*, *41*, 1085–1092, doi:10.1002/2013GL059132.
- Li, X., and M. A. Temerin (2001), The electron radiation belt, *Space Sci. Rev.*, *95*, 569–581.
- Lorentzen, K. R., M. D. Looper, and J. B. Blake (2001), Relativistic electron microbursts during the GEM storms, *Geophys. Res. Lett.*, *28*, 2573–2576, doi:10.1029/2001GL012926.
- McRae, W. M., and N. R. Thomson (2000), VLF phase and amplitude: Daytime ionospheric parameters, *J. Atmos. Sol. Terr. Phys.*, *62*(7), 609–618.
- Meredith, N. P., R. B. Horne, M. A. Clilverd, D. Horsfall, R. M. Thorne, and R. R. Anderson (2006a), Origins of plasmaspheric hiss, *J. Geophys. Res.*, *111*, A09217, doi:10.1029/2006JA011707.
- Meredith, N. P., R. B. Horne, S. A. Glauert, R. M. Thorne, D. Summers, J. M. Albert, and R. R. Anderson (2006b), Energetic outer zone electron loss timescales during low geomagnetic activity, *J. Geophys. Res.*, *111*, A05212, doi:10.1029/2005JA011516.
- Neal, J. J., C. J. Rodger, M. A. Clilverd, N. R. Thomson, T. Raita, and T. Ulich (2015), Long-term determination of energetic electron precipitation into the atmosphere from AARDDVARK subionospheric VLF observations, *J. Geophys. Res. Space Physics*, *120*, 2194–2211, doi:10.1002/2014JA020689.
- O’Brien, T. P., and M. B. Moldwin (2003), Empirical plasmopause models from magnetic indices, *Geophys. Res. Lett.*, *30*(4), 1152, doi:10.1029/2002GL016007.
- O’Brien, T. P., M. D. Looper, and J. B. Blake (2004), Quantification of relativistic electron microburst losses during the GEM storms, *Geophys. Res. Lett.*, *31*, L04802, doi:10.1029/2003GL018621.
- Reeves, G. D., K. L. McAdams, and R. H. W. Friedel (2003), Acceleration and loss of relativistic electrons during geomagnetic storms, *Geophys. Res. Lett.*, *30*(10), 1529, doi:10.1029/2002GL016513.
- Rodger, C. J., O. A. Molchanov, and N. R. Thomson (1998), Relaxation of transient ionization in the lower ionosphere, *J. Geophys. Res.*, *103*(A4), 6969–6975, doi:10.1029/98JA00016.
- Rodger, C. J., M. A. Clilverd, and R. J. McCormick (2003), Significance of lightning-generated whistlers to inner radiation belt electron lifetimes, *J. Geophys. Res.*, *108*(A12), 1462, doi:10.1029/2003JA009906.
- Rodger, C. J., M. A. Clilverd, N. R. Thomson, R. J. Gamble, A. Seppälä, E. Turunen, N. P. Meredith, M. Parrot, J. A. Sauvaud, and J.-J. Berthelier (2007), Radiation belt electron precipitation into the atmosphere: Recovery from a geomagnetic storm, *J. Geophys. Res.*, *112*, A11307, doi:10.1029/2007JA012383.
- Rodger, C. J., M. A. Clilverd, J. Green, and M.-M. Lam (2010a), Use of POES SEM-2 observations to examine radiation belt dynamics and energetic electron precipitation in to the atmosphere, *J. Geophys. Res.*, *115*, A04202, doi:10.1029/2008JA014023.
- Rodger, C. J., M. A. Clilverd, A. Seppälä, N. R. Thomson, R. J. Gamble, M. Parrot, J.-A. Sauvaud, and T. Ulich (2010b), Radiation belt electron precipitation due to geomagnetic storms: Significance to middle atmosphere ozone chemistry, *J. Geophys. Res.*, *115*, A11320, doi:10.1029/2010JA015599.

- Rodger, C. J., A. J. Kavanagh, M. A. Clilverd, and S. R. Marple (2013), Comparison between POES energetic electron precipitation observations and riometer absorptions: Implications for determining true precipitation fluxes, *J. Geophys. Res. Space Physics*, *118*, 7810–7821, doi:10.1002/2013JA019439.
- Rozanov, E., L. Callis, M. Schlesinger, F. Yang, N. Andronova, and V. Zubov (2005), Atmospheric response to NO_y source due to energetic electron precipitation, *Geophys. Res. Lett.*, *32*, L14811, doi:10.1029/2005GL023041.
- Santolik, O., D. A. Gurnett, J. S. Pickett, M. Parrot, and N. Cornilleau-Wehrin (2006), Five years of investigation of whistler-mode chorus using the measurements of the Cluster spacefleet, in *Proceedings of the Cluster and Double Star Symposium-5th Anniversary of Cluster in Space*, *Eur. Space Agency Spec. Publ.*, edited by K. Fletcher, Noordwijk, Netherlands.
- Seppälä, A., M. A. Clilverd, and C. J. Rodger (2007), NO_x enhancements in the middle atmosphere during 2003–2004 polar winter: Relative significance of solar proton events and the aurora as a source, *J. Geophys. Res.*, *112*, D23303, doi:10.1029/2006JD008326.
- Seppälä, A., C. E. Randall, M. A. Clilverd, E. Rozanov, and C. J. Rodger (2009), Geomagnetic activity and polar surface air temperature variability, *J. Geophys. Res.*, *114*, A10312, doi:10.1029/2008JA014029.
- Simon Wedlund, M., M. A. Clilverd, C. J. Rodger, K. Cresswell-Moorcock, N. Cobbett, P. Breen, D. Danskin, E. Spanswick, and J. V. Rodriguez (2014), A statistical approach to determining energetic outer radiation-belt electron precipitation fluxes, *J. Geophys. Res. Space Physics*, *119*, 3961–3978, doi:10.1002/2013JA019715.
- Smith, E. J., A. M. A. Frandsen, B. T. Tsurutani, R. M. Thorne, and K. W. Chan (1974), Plasmaspheric hiss intensity variations during magnetic storms, *J. Geophys. Res.*, *79*, 2507, doi:10.1029/JA079i016p02507.
- Summers, D., B. Ni, and N. P. Meredith (2007), Timescales for radiation belt electron acceleration and loss due to resonant wave-particle interactions: 2. Evaluation for VLF chorus, ELF hiss, and electromagnetic ion cyclotron waves, *J. Geophys. Res.*, *112*, A04207, doi:10.1029/2006JA011993.
- Thomson, N. R., and W. M. McRae (2009), Nighttime ionospheric *D* region: Equatorial and nonequatorial, *J. Geophys. Res.*, *114*, A08305, doi:10.1029/2008JA014001.
- Thomson, N. R., M. A. Clilverd, and W. M. McRae (2007), Nighttime ionospheric *D* region parameters from VLF phase and amplitude, *J. Geophys. Res.*, *112*, A07304, doi:10.1029/2007JA012271.
- Thomson, N. R., M. A. Clilverd, and C. J. Rodger (2011), Daytime midlatitude *D* region parameters at solar minimum from short-path VLF phase and amplitude, *J. Geophys. Res.*, *116*, A03310, doi:10.1029/2010JA016248.
- Thorne, R. M., T. P. O'Brien, Y. Y. Shprits, D. Summers, and R. B. Horne (2005), Timescale for MeV electron microburst loss during geomagnetic storms, *J. Geophys. Res.*, *110*, A09202, doi:10.1029/2004JA010882.
- Turunen, E., P. T. Verronen, A. Seppälä, C. J. Rodger, M. A. Clilverd, J. Tamminen, C. F. Enell, and T. Ulich (2009), Impact of different precipitation energies on NO_x generation during geomagnetic storms, *J. Atmos. Sol. Terr. Phys.*, *71*, 1176–1189, doi:10.1016/j.jastp.2008.07.005.
- Verronen, P. T., C. J. Rodger, M. A. Clilverd, and S. Wang (2011), First evidence of mesospheric hydroxyl response to electron precipitation from the radiation belts, *J. Geophys. Res.*, *116*, D07307, doi:10.1029/2010JD014965.
- Voss, H. D., M. Walt, W. L. Imhof, J. Mobilia, and U. S. Inan (1998), Satellite observations of lightning-induced electron precipitation, *J. Geophys. Res.*, *103*(A6), 11,725–11,744, doi:10.1029/97JA02878.
- Wait, J. R., and K. P. Spies (1964), *Characteristics of the Earth-Ionosphere Waveguide for VLF Radio Waves*, *NBS Tech. Note 300*, p. 93, Natl. Bur. of Stand., Gaithersburg, Md.
- Whittaker, I. C., M. A. Clilverd, and C. J. Rodger (2014), Characteristics of precipitating energetic electron fluxes relative to the plasmapause, *J. Geophys. Res. Space Physics*, *119*, 8784–8800, doi:10.1002/2014JA020446.
- Xiao, F., et al. (2014), Chorus acceleration of radiation belt relativistic electrons during March 2013 geomagnetic storm, *J. Geophys. Res. Space Physics*, *119*, 3325–3332, doi:10.1002/2014JA019822.